Phase diagrams for cohesive particle mixing and segregation

Hongming Li and J. J. McCarthy*
Department of Chemical and Petroleum Engineering, University of Pittsburgh, Pittsburgh, Pennsylvania 15261, USA
(Received 30 April 2004; revised manuscript received 30 September 2004; published 28 February 2005)

By taking a discrete view of cohesion, we develop a particle-level model which can accurately predict the extent of particle mixing and segregation in cohesive (wet) granular systems. Our model is based on a discrete characterization tool and is used to generate phase diagrams of the predicted particle behavior. These phase diagrams exhibit both mixed and segregated phases where the boundary is determined by the mechanical and surface properties of the particles, such that manipulation of surface properties and/or size/density ratios provides a method to control cohesive particle mixing and segregation. A detailed description of the phase diagram development process as well as quantitative validation of the theoretical results are reported here.

DOI: 10.1103/PhysRevE.71.021305 PACS number(s): 45.70.Mg, 64.75.+g, 81.30.Mh

I. INTRODUCTION

Mixing of granular materials is of considerable practical importance to many industries, such as pharmaceutical, chemical, food, and construction, and has intrigued researchers for years [1–5]. It is well known that mixing is invariably limited by the tendency for granular materials to simultaneously demix or segregate due to differences in size, density, shape, etc. [6,7], and the interplay of mixing and segregation is critical to the analysis and design of industrial mixing operations [8].

Despite significant advances in our understanding of the role of moisture in granular flows [9–16], much remains to be done. In particular, while it has been long believed that cohesion mitigates segregation, the origin of this phenomenon has been elusive [2,17]. Nevertheless, recent work focusing on the effect of varying moisture level on segregation has shown a rich behavior both as a function of forcing velocity [11] and interstitial liquid viscosity [9].

In this work, our group focuses on a fixed volume (percent) of interstitial liquid and differing particle properties. As will be discussed, our particle flow is sufficiently gentle as to be located within the "mixing" phase of Geromichalos, although a variety of mixing/segregation behavior is observed as particle properties are varied. We develop a microscopic (particle-level) model which we use to connect the macroscopic properties of the granular mixing/segregation to the effects of interparticle forces. In earlier work, we developed a simple discrete-based tool to characterize cohesive (liquid-bridging induced) granular materials [18]. Here, we use an extended tool applicable to binary particle systems, so that we can determine phase diagrams which exhibit both mixed and segregated phases for particle systems [12]. The boundary of the phases depends on the mechanical and surface properties of the particles [12]. By using these phase diagrams we are able to predict the extent of mixing for given combinations of particles, and provide a method for controlling cohesive particle mixing. To support the theory various experiments and simulations are conducted in a simple, industrially relevant, granular flow, a tumbler.

*Electronic address: jjmcc@pitt.edu

II. COHESIVE MIXING MODEL

A. Characterization tool

While the ubiquitous sink of granular thermal energy—inelastic collisions—makes metastable or nonequilibrium states quite commonplace in particulate systems [19], a continuous input of energy supply (here, the rotated tumbler) can be used to exactly balance the energy lost to inelastic collisions. As a result, the system may eventually reach an asymptotic state, where the reversible process between mixing and segregation cancels and the particle distribution is essentially invariant. It is at this point that our model is applicable. The basis of the model is that, in the asymptotic state, the distribution of particles in a cohesive system will depend almost wholly on the relative importance of the various forces acting on the particles. Therefore by examining the magnitude of the cohesion force (here liquid-bridge induced) relative to other relevant forces, we can quantify and elucidate the impact of the cohesion force on the system.

As a simple way to obtain an unquenched, asymptotic granular state, we use a half filled tumbler. When this geometry is operated in the continuous flow or rolling regime, the bulk of the bed undergoes a solid-body rotation by following the cylinder motion. Near the surface, the particles flow downward along the surface in a thin layer continuously (i.e., without avalanches) until they enter the bed again, and the process repeats [20,21]. Under these conditions, mixing occurs almost solely due to collision-induced diffusion in the thin surface layer [8]. After many revolutions, the particle distribution in the bed remains time invariant and the system is assumed to reach its asymptotic state. In our cohesive trials, we add a small but consistent amount of interstitial liquid to the bed ($\approx$1% volume). In all cases, we operate the tumbler in the continuous flow regime, yet at a sufficiently slow rotation rate that the shearing force is considerably smaller than the particle weight, and the average velocity of the beads limits the kinetic energy to the viscoplastic regime [11]. The relevant forces acting on the particles therefore include the cohesion force (F_c) and the particle weight (F_w). The characterization tool that is the basis of our model, in this case, is the granular bond number (Bo_g) which is defined as a ratio of the maximum F_c to F_w. For a monodisperse system [18] it is given as

$$\mathrm{Bo}_g = \frac{F_c}{F_w} = \frac{2\pi\gamma R}{\frac{4}{3}\pi g R^3 \rho}, \tag{1}$$

where γ is the interstitial fluid's surface tension, R and ρ are the radius and density of particle, respectively, and g is the acceleration due to gravity. It should be noted that this tool, and in fact this work, is geared toward systems where the liquid bridges act only pairwise (i.e., the system is in the pendular regime).

B. Phase diagram

In order to use the granular bond number to examine the impact of cohesion on particle mixing/segregation, we extend the Bo_g for a homogeneous system to binary systems where particles have different sizes, densities, and/or wetting characteristics as

$$\mathrm{Bo}_g = \frac{2\pi\gamma R_e(\cos\theta)_{min}}{\frac{4}{3}\pi g(R^3\rho)_{min}} = \frac{3\gamma R_e(\cos\theta)_{min}}{2g(R^3\rho)_{min}}, \tag{2}$$

where γ is the interstitial fluid's surface tension, $(R^3\rho)_{min}$ is the smaller of the two masses to represent the fact that a less massive particle's motion will be dominated by the more massive particle (i.e., it will behave as a guest), θ is the wetting angle, R_e is the geometric mean radius $[R_e = 2R_1R_2/(R_1+R_2)]$, and differing wetting characteristics are incorporated simply by using the larger value of θ (or the smaller value of $\cos\theta$).

The values of the Bo_g for each potential pair of particles, i and j, within the system (i.e., for a binary system, the $\mathrm{Bo}_{g11}, \mathrm{Bo}_{g22}$, and Bo_{g12}, where 2 is defined as the larger of the particles) need to then be compared. It should be noted that this approach necessarily limits our applicable range of size ratios for two reasons. First, as the size ratio becomes (infinitely) small, maintaining the bed in the pendular regime will become impossible. Second, directly comparing pairwise particle interactions neglects both multiparticle interactions as well as the reality that for small size ratios the probability of the three types of pairwise interactions may be very different (so some scaled comparison would be warranted). Nevertheless, as can be seen in Sec. IV, this simple approach works well even down to size ratios of 0.25 (i.e., interaction probability ratios of 16 to 1).

Comparing the magnitudes of these Bo_{gij} leads to two dimensionless groups:

$$\Re_1 = \frac{\mathrm{Bo}_{g11}}{\mathrm{Bo}_{g12}} = \frac{R_1+R_2}{2R_2}\frac{\cos\theta_1}{(\cos\theta_1,\cos\theta_2)_{min}}\frac{(R_1^3\rho_1,R_2^3\rho_2)_{min}}{R_1^3\rho_1}, \tag{3}$$

$$\Re_2 = \frac{\mathrm{Bo}_{g22}}{\mathrm{Bo}_{g12}} = \frac{R_1+R_2}{2R_1}\frac{\cos\theta_2}{(\cos\theta_1,\cos\theta_2)_{min}}\frac{(R_1^3\rho_1,R_2^3\rho_2)_{min}}{R_2^3\rho_2}, \tag{4}$$

which can be rewritten by defining $\alpha=\rho_1/\rho_2$, $\beta=R_1/R_2$, and $\lambda=\cos\theta_1/\cos\theta_2$, yielding

$$\Re_1 = \frac{\mathrm{Bo}_{g11}}{\mathrm{Bo}_{g12}} = \frac{\beta+1}{2}\frac{\lambda}{(\lambda,1)_{min}}\frac{(\alpha\beta^3,1)_{min}}{\alpha\beta^3}, \tag{5}$$

$$\Re_2 = \frac{\mathrm{Bo}_{g22}}{\mathrm{Bo}_{g12}} = \frac{\beta+1}{2\beta}\frac{1}{(\lambda,1)_{min}}\frac{(\alpha\beta^3,1)_{min}}{1}. \tag{6}$$

In order to determine the mixing behavior we can then *analytically* determine the locations of the phase boundaries of our mixing/segregation diagram by identifying where in the parameter space of size ratio (β), density ratio (α), and wetting angle ratio (λ) differing hierarchies of Bo_{gij} are observed.

The following cases may be observed:
If $\alpha\beta^3>1$,

$$1<\Re_1, 1<\Re_2, \quad \lambda > \frac{2\alpha\beta^3}{1+\beta},$$

$$\Re_1<1<\Re_2, \quad \lambda < \frac{2\alpha\beta^3}{1+\beta}. \tag{7}$$

If $\alpha\beta^3<1$,

$$\Re_1<1, \Re_2<1, \quad \frac{(\beta^3+\beta^2)\alpha}{2} < \lambda < \frac{2}{1+\beta},$$

$$\Re_1<1<\Re_2, \quad \lambda < \frac{(\beta^3+\beta^2)\alpha}{2},$$

$$\Re_2<1<\Re_1, \quad \lambda > \frac{2}{1+\beta}. \tag{8}$$

In the case of $\alpha\beta^3>1$ (i.e., the smaller particle is more massive than the larger particle), $\Re_2>1$ is always true for any combination of particle properties (i.e., size, density, and/or surface characteristics). This implies that the interaction of the two dissimilar particles (i.e., the "mixing" interaction) is always weaker than the interaction of the two largest particles (see Fig. 1). In fact, for some values of λ, the dissimilar particles interaction is the *weakest* of the three possible interactions. We expect that this region of parameter space will therefore always favor segregation as larger particles cluster together and exclude smaller ones. This suggests that cohesion here will lead to a mechanism of segregation and ultimately *more* segregation than would be achieved in the dry case.

In contrast, in the case of $\alpha\beta^3<1$ (i.e., the small particle is less massive), when $\alpha(\beta^3+\beta^2)/2<\lambda<2/(1+\beta)$, both $\Re_1$ and $\Re_2$ are less than 1. This indicates that the interaction between dissimilar particles is the strongest, therefore favoring intimate particle mixing. Systems that lie in this region of parameter space are expected to be more mixed than the corresponding dry experiment. For other values of λ, however, $\Re_2>1$ or $\Re_1>1$, so that in this region, as well, we expect some instances of cohesion-enhanced segregation.

It is instructive at this point to examine in detail why hierarchies of properly scaled cohesive force (i.e., Bo_g) are used as opposed to simply comparing that of the unscaled F_c. Consider particles of the same density and surface properties, but differing diameters. Clearly, the largest unscaled cohesive force will be found to exist between two larger particles ($F_c \propto R_e$). Nevertheless, the particle sizes may be chosen in

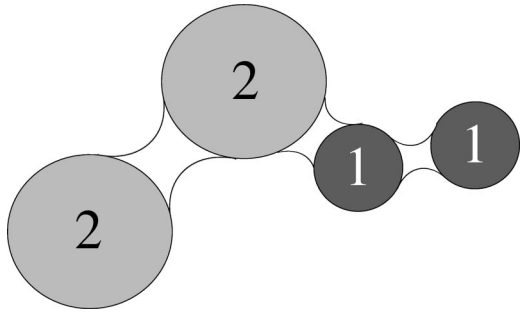

FIG. 1. Schematic demonstration of the possible interactions between particles in a binary cohesive system, leading to Bo_{g11}, Bo_{g22}, and Bo_{g12}.

such a way that $\mathrm{Bo}_{g_{22}} < 1 < \mathrm{Bo}_{g_{12}}$. In this case, despite the fact that the unscaled cohesive force is strongest between the two large particles (i.e., $F_{c_{22}} > F_{c_{12}}$), the larger particles will not adhere to each other, yet the smaller ones will adhere to the larger ones (a simple physical example might be sand sticking to a bowling ball) [12]. In fact, under these conditions—particles differing only in size—it is easily shown that the mixing interaction is always most significant (largest Bo_g) despite the fact that the unscaled F_c values may lead one to think otherwise.

The implications of combining Eqs. (7) and (8) are best visualized by phase diagrams, which outline regions of mitigated (*M* phase) and enhanced (*E* phase) segregation for particle mixing/segregation. The definitions of these phases are based on the values of $\Re_1$ and $\Re_2$, as discussed above; that is, values of $\Re_i$ greater than 1 lead to segregation. Figure 2 shows the phase diagrams for the case of $\alpha = 1$ (left), $\alpha = 0.56$ (right with both light and dark gray *M* phase), and $\alpha = 1.8$ (right with only dark gray *M* phase). In both plots, the white region corresponds to the *E* phase where $\Re_i > 1$ for either $i = 1,2$ or both, while the gray region corresponds to the *M* phase where both $\Re_i$ values are less than 1. From the right-most plot it is clear that, in general, varying the density ratio causes a relative change in the size of the *M* and *E* phases—the *M* phase grows when the smaller particle is less dense and shrinks when it is more dense. Finally, in anticipation of using the model for quantitative analysis of the extent of segregation, the left-most plot in Fig. 2 shows dashed lines corresponding to various values of $\Re_i > 1$. It should be noted that on the far right axis (where the size ratio is equal to 1), the value of $\Re_i$ for λ is equal to that of $1/\lambda$, as the identity of particle 2 (the larger one) is not defined.

III. EXPERIMENTAL SETUP

We use binary mixtures of spherical particles—glass and/or acrylic—in half filled, pseudo-two-dimensional tumbler mixers. The mixer is made of a glass petri dish (which is treated with a hydrophobic silane to reduce adhesion to the surfaces) and is cylindrical in shape with roughly 14 cm diameter and 2 cm depth. The total available volume of the petri dish is 308 mL. In each experiment, the tumbler is filled half way (approximately 150 mL). The particles are initially completely segregated, with component *i* being contained in the lower left quarter of the tumbler and component *j* in the lower right quarter. We conduct experiments first with dry beads, then repeat the experiment under the same conditions except with the addition of a small amount of distilled water ($\approx 1\%$ by volume). After approximately thirty revolutions the system reaches the asymptotic state. The digitized images of the particle distribution at both initial and asymptotic states are taken for later comparison and image processing to obtain qualitative and quantitative information. The effect of the cohesion force can be elucidated with an examination of the difference in the pictures at asymptotic states between the dry and wet case. Experimentally we restrict the rotation speed such that it is sufficiently small (6–9 rpm) to assure the system is in the rolling regime and that the cohesion is primarily dictated by the granular bond number Bo_g.

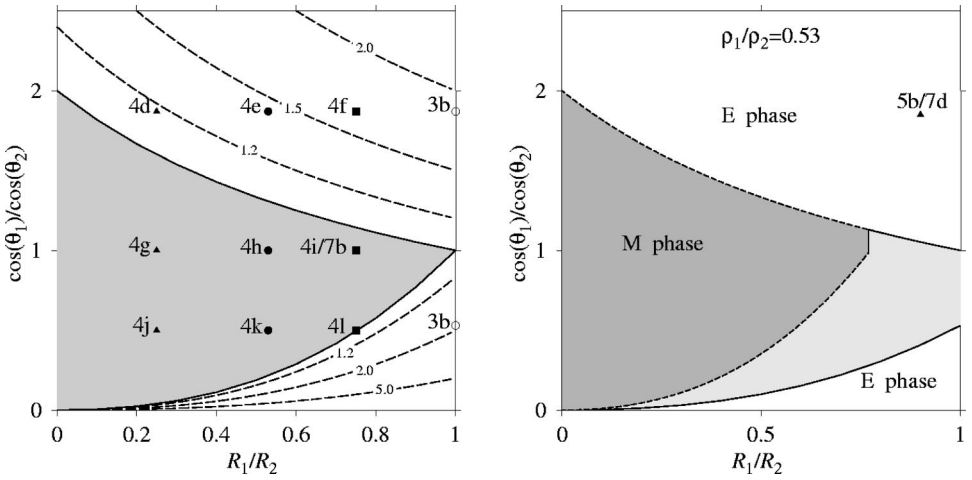

FIG. 2. Phase diagrams for binary cohesive systems. Phase diagrams are a function of the ratios of sizes, densities, and values of the cosine of the wetting angles. Left: Phase diagram for the systems with $\rho_1/\rho_2 = 1$. Solid lines depict phase boundaries, while dashed lines show contours of the larger $\Re_i$ values. Right: The size of the *M* phase for a density ratio of 0.56 grows, and the phase boundary is shown as a solid line; while that of the inverse case (density ratio of 1.78) shrinks, the phase boundary is shown as a dashed line, i.e., the lighter gray region becomes part of the *E* phase.

TABLE I. List of experiments conducted.

Expt.	R_1 (mm)	R_2 (mm)	ρ_1 (g/cm^3)	ρ_2 (g/cm^3)	θ_1	θ_2	Phase
3*a*	0.4	0.4	2.5[a]	2.5			dry
3*b*	0.4	0.4	2.5	2.5	20°	60°	*E*
4*a*	0.25	1.0	2.5	2.5			dry
4*d*	0.25	1.0	2.5	2.5	20°	60°	*E*
4*g*	0.25	1.0	2.5	2.5	20°	20°	*M*
4*j*	0.25	1.0	2.5	2.5	60°	20°	*M*
4*b*	0.4	0.75	2.5	2.5			dry
4*e*	0.4	0.75	2.5	2.5	20°	60°	*E*
4*h*	0.4	0.75	2.5	2.5	20°	20°	*M*
4*k*	0.4	0.75	2.5	2.5	60°	20°	*M*
4*c*/7*a*	0.75	1.0	2.5	2.5			dry
4*f*	0.75	1.0	2.5	2.5	20°	60°	*E*
4*i*/7*b*	0.75	1.0	2.5	2.5	20°	20°	*M*
4*l*	0.75	1.0	2.5	2.5	60°	20°	*M*
5*a*	0.9	1.0	1.4[b]	2.5			dry
5*b*	0.9	1.0	1.4	2.5	50°	70°	*E*
7*c*	0.9	1.0	1.4	2.5			dry
7*d*	0.9	1.0	1.4	2.5	20°	60°	*E*

[a]Material: soda lime glass.
[b]Material: acrylic.

All glass beads are initially soaked in a dilute HF solution both to clean the surfaces as well as produce approximately uniform surface roughnesses. Depending on the experiment, half are further treated with a surface-modifying hydrophilic silane (and a trace amount of fluorescent silane following a procedure detailed in Ref. [22]) and the other half with a hydrophobic silane (and a trace amount of colored fluorescent silane). As a result, the particles have wetting angles of $\theta \approx 20°$ (hydrophilic) and $\theta \approx 60°$ (hydrophobic), respectively. The wetting angles of beads are measured by inspection of magnified images of roughly microliter sized droplets on actual particle surfaces. The range of particle mechanical and surface properties examined in these experiments are summarized in Table I.

IV. EXPERIMENTAL RESULTS AND DISCUSSION

A. Qualitative analysis

In all the dry cases (see Table I, experiments 3*a*,4*a*,4*b*,4*c*,5*a*), the segregation by density will force the less dense particles to the periphery and the more dense particles to the inner core, while the segregation by size will promote larger particles migrating to the periphery and smaller particles to the inner core [2]. All the dry systems will end up with the particles segregated but with differing segregation distribution with the exception of experiment 3*a* (Table I) where the particles are mechanically identical, but have different wetting angles so that they are perfectly mixed at the asymptotic state, when dry.

As discussed in detail below, the results from the wet experiments show a dramatic change of particle distribution (i.e., mixing/segregation) relative to that of the dry cases. Each change is both qualitatively and quantitatively in agreement with the predictions of our model.

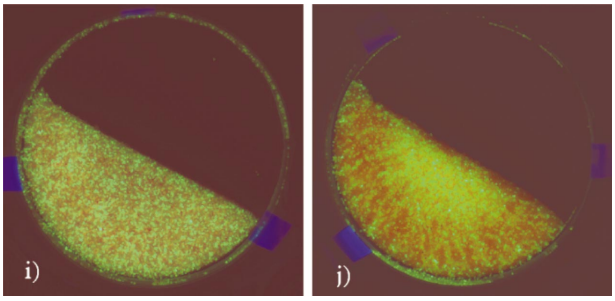

FIG. 3. (Color) Varying wetting angles. (a) Particles with differing surface properties (red hydrophilic and green hydrophobic) but otherwise identical in all other respects [Fig. 2, point(s) 3*b*] will mix perfectly when tumbled dry; however, (b) when interstitial water is added, they will instead segregate.

1. Varying wetting angles

The particles in system 3*b* ($\alpha=1$, $\beta=1$, $\lambda=1.88$ or 0.53) have the same size and density but different wetting angles (see Table I, experiment 3*b*) so that it represents the *E* phase [point(s) 3*b* in Fig. 2; note that the "larger" particle is undefined in this case]. While the particles are perfectly mixed in the dry case [Fig. 3(a)], our model predicts that adding water will make the particles segregate more than in the dry case. Figure 3(b) (wet case) shows that there are more green beads (here, hydrophobic) clustered in the center of the tumbler. This can be easily understood in this way: since the weights of both types of particles are the same, the smaller wetting angle between hydrophilic beads (red/orange) yields a larger cohesion force, and thus a bigger granular bond number (Bo_g). The hydrophilic particles (red) then preferentially cluster together and migrate toward the outside.

2. Varying wetting angles and size ratios

We next conduct three sets of experiments with varying particle size ratio in addition to the wetting angle (Fig. 4). One set of experiments is with glass beads of 0.25 mm (radius) along with 1.0 mm—i.e., the size ratio is 0.25 (Table I, experiments 4*a*,4*d*,4*g*,4*j*; Fig. 2). The second set of experiments is with glass beads of 0.4 mm along with 0.75 mm—i.e., the size ratio is 0.53 (Table I, experiments 4*b*,4*e*,4*h*,4*k*; Fig. 2). The last set of experiments is with glass beads of 0.75 mm along with 1.0 mm—i.e., the size ratio is 0.75 (Table I, experiments 4*c*,4*f*,4*i*,4*l*; Fig. 2).

It is obvious that, for all three size ratios, the dry case leads to strong radial segregation due to size differences [Figs. 4(a)–4(c)]. The smaller particles stay at the center (dark) areas while the larger ones remain at the periphery. When the small particle is more hydrophilic (here, green), the systems represent the *E* phase (points 4*d*, 4*e*, and 4*f* in Fig. 2). We therefore expect that the segregation achieved in the dry cases will be enhanced (or remain strong) by adding water. While Figs. 4(d)–4(f) confirm our prediction, the macroscopic segregation patterns are beyond our expectation, but

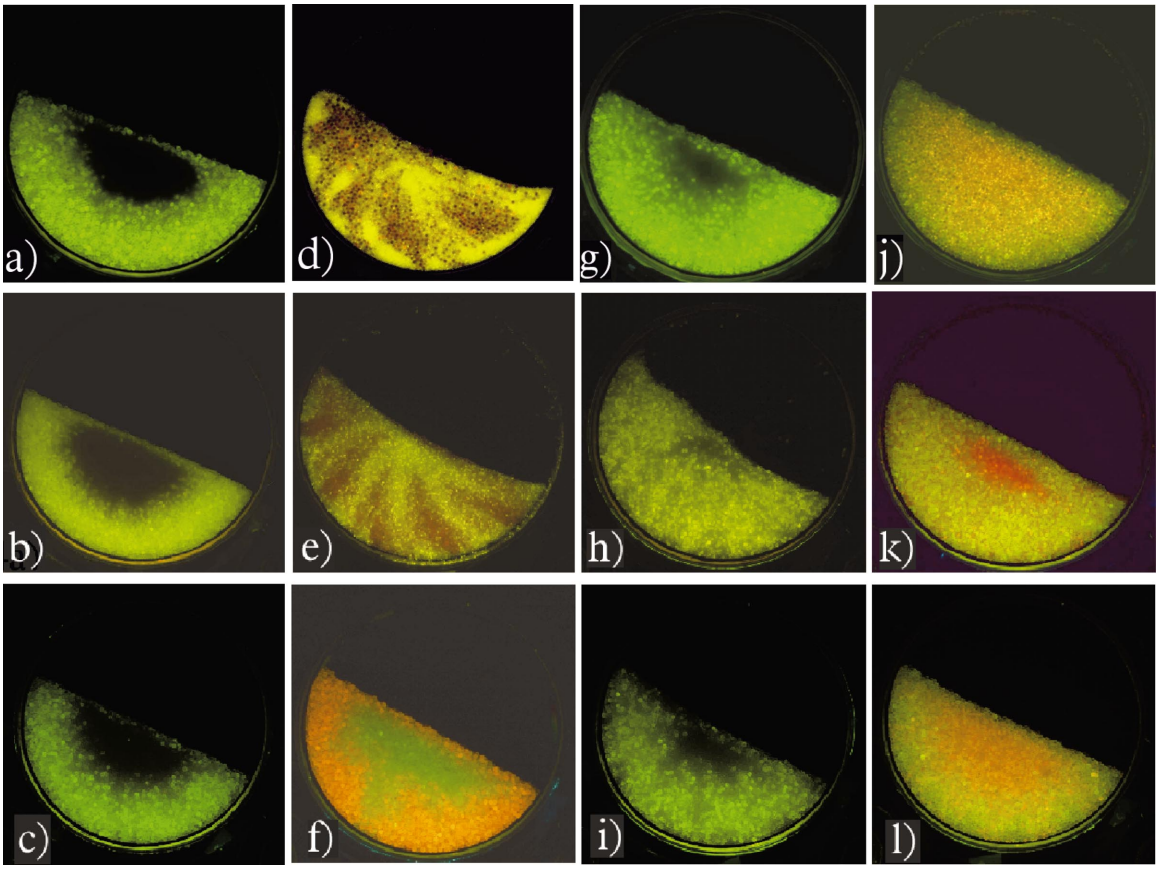

FIG. 4. (Color) Varying size ratio and wetting angle. From top to bottom the rows correspond to size ratios of 0.25, 0.53, and 0.75, respectively. From left to right the images represent results when dry, (a)–(c); wet with the smaller particle (green) being more hydrophilic, (d)–(f); wet with both particles hydrophilic, (g)–(i); and wet with the smaller particle (red/orange) being more hydrophobic, (j)–(l). Results are in agreement with the predictions from theory (Fig. 2).

may be related to the time varying surface angle resulting from the difference in cohesion between the two materials [23]. When the particles have almost identical wetting angles, the systems represent the *M* phase (points 4*g*, 4*h*, and 4*i*, Fig. 2). Figures 4(g)–4(i) show that the core (dark) areas in all experiments shrink after adding water, i.e., particles mix more than in the dry cases, as expected. Finally, when the larger particles are more hydrophilic (points 4*j*, 4*k*, and 4*l* in Fig. 2), the 0.25 and 0.53 cases remain firmly in the *M* phase and mix more than in the dry case [i.e., core (red) area shrinks], however, since the 0.75 case lies near the phase boundary, the experiment is essentially unaffected by cohesion (see Figs. 4(j)–4(l)] [12].

3. Varying density ratio, size ratio and wetting angles

Finally, we vary the density ratio, size ratio, and wetting characteristics at the same time. Figure 5 shows the results for the case $\alpha=0.56$, $\beta=0.9$, and $\lambda=1.88$ (i.e., point 5*b* in Fig. 2). The asymptotic distribution for dry particles represents only mild radial segregation as the density and size effects compete and almost cancel each other [see Fig. 5(a)]. In the wet case, however, the same initial condition instead evolves to a more segregated state as predicted [Fig. 5(b)].

B. Quantitative analysis

Quantitatively, we process the digitized images of the asymptotic state from both the dry and wet cases to extract concentration maps. In the digitized images each pixel is identified as its own RGB value that represents the degree of red, green, and blue. A threshold value of red to green intensity is determined from the known volume ratio and positions of the initial condition. The images are then segmented so that mixing measurement calculations may be performed. A mixing measure (*IS*), essentially the standard deviation of the concentration, is calculated from multiple spot concentration measurements as

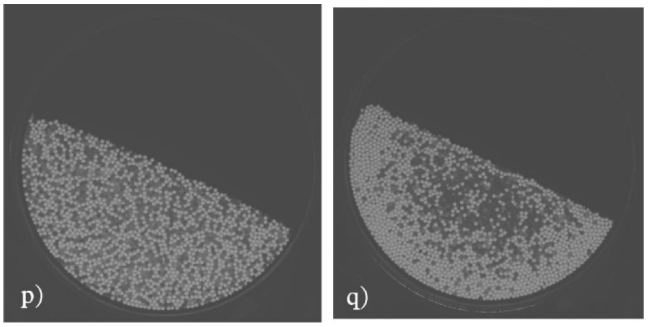

FIG. 5. Varying density ratios. When particles of density ratio of 0.56, size ratio 0.9 and wetting angle ratio 1.88 (Fig. 2, point 5*b*) are tumbled: (5*a*) dry, they will segregate radially only slightly; (5*b*) add water and they segregate more profoundly.

$$IS = \sqrt{\frac{\sum_{i=1}^{N} (C - C_{avg})^2}{N-1}}, \tag{9}$$

where N is the number of useful cells, C is the concentration of red or green pixels in a designated cell, and C_{avg} is the average concentration of red or green pixels in the entire image. Table II lists all the *IS* values for the experiments conducted, as well as the percentage change from the corresponding dry cases, which are calculated as

$$\text{change } (\%) = \frac{IS_{dry} - IS_{wet}}{IS_{dry}} \times 100\,\%\,. \tag{10}$$

A positive change means the system is more mixed than in the dry case while a negative change means more segregated.

Figure 6 shows the variation of the mixing extent change [Eq. (10)] as a function of $\Re_i$. As is evident from the development of the phase diagrams, the *maximum* value of $\Re_i$ is the critical value for the case of cohesion-enhanced segregation (i.e., where one of $\Re_i > 1$). By analogy, one might argue that the critical value for cohesion-enhanced mixing is that of the *minimum* $\Re_i$. In Fig. 6, we show both values of $\Re_i$, but highlight the expected critical value as a solid symbol. If one were to follow the critical values, we would obtain a rotated sigmoidal dependency, whereas tracking the average value would yield roughly a linear dependence. Our theory would predict that all experiments should lie in either the upper left or lower right quadrants (as our critical values do).

V. DEM SIMULATION

To further test our theory, particle dynamics simulations are performed. Particle dynamics has been quite successful in simulating granular materials, yielding insight into such diverse phenomena as force transmission [24], agglomeration formation and breakage [25], and segregation of cohesionless materials [26]. It captures the bulk flow of the material via simultaneous integration of the interaction forces between individual pairs of particles, and the particle trajectories are obtained via explicit solution of Newton's equation of motion for every particle [27]. While the forces in the system typically include only a contact force (normal repulsion), tangential friction, and gravity, additional particle interaction forces (e.g., capillary force and van der Waals force, etc.) can be easily added. In this work, the collisional forces are modeled after the work of Hertz and Mindlin [28]. The cohesive forces, which arise from liquid bridging, are modeled after the work of Lian and Thornton [29,30]. For simplicity, bridges form at the instant of interparticle contact and persist until the separation between surfaces is sufficient to rupture the bridge. Also, the liquid content of each bridge is assumed to be a constant, here taken as 0.1% of the volume of the largest particle. Both of these simplifications are consistent with existing literature [30–32] and have compared favorably with experiment.

We performed two sets of simulations to compare to the experimental results. One set of simulations (cases 7*a* and 7*b*) is conducted using a computational analogue of the cases 4*c* and 4*i*, i.e., the glass beads of 0.75 mm (radius) along with 1.0 mm (Table I); however, the particle stiffness is lowered to facilitate more rapid computations without affecting kinematic results [33]. As in the experiment 4*c* [Fig. 4(c)], the particles segregate strongly when dry [Fig. 7(a)], yet become more mixed when wet [Fig. 7(b); point 7*b* in Fig. 2].

The other set of simulations (case 7*c* and 7*d*, Table I) is conducted with the smaller particle being less dense ($\alpha = 0.56$), and more hydrophilic ($\theta \approx 20°$ versus $\theta \approx 60°$). Here we chose slightly different absolute values of the wetting angles that nevertheless yield essentially the same wetting

TABLE II. Quantitative analysis of the experimental results.

	Dry case	Wet case	Wet case	Wet case
	3*a*			3*b*(*s*)
$\Re_1$				1.9 (1)
$\Re_2$				1 (1.9)
IS	0.16			0.24
IS change %				−54%
	4*a*	4*d*	4*g*	4*j*
$\Re_1$		1.2	0.63	0.63
$\Re_2$		0.04	0.04	0.07
IS	0.356	0.361	0.25	0.26
IS change %		−1.5%	29%	27%
	4*b*	4*e*	4*h*	4*k*
$\Re_1$		1.4	0.77	0.77
$\Re_2$		0.22	0.22	0.41
IS	0.37	0.39	0.21	0.31
IS change %		−5.8%	44%	18%
	4*c*	4*f*	4*i*	4*l*
$\Re_1$		1.6	0.88	0.88
$\Re_2$		0.49	0.49	0.93
IS	0.39	0.41	0.30	0.37
IS change %		−5.9%	24%	4.6%
	5*a*	5*b*		
$\Re_1$		1.8		
$\Re_2$		0.43		
IS	0.27	0.35		
IS change %		−29%		
	7*a*		7*b*	
$\Re_1$			0.88	
$\Re_2$			0.49	
IS	0.39		0.30	
IS change %			23%	
	7*c*	7*d*		
$\Re_1$		1.8		
$\Re_2$		0.43		
IS	0.25	0.33		
IS change %		−29%		

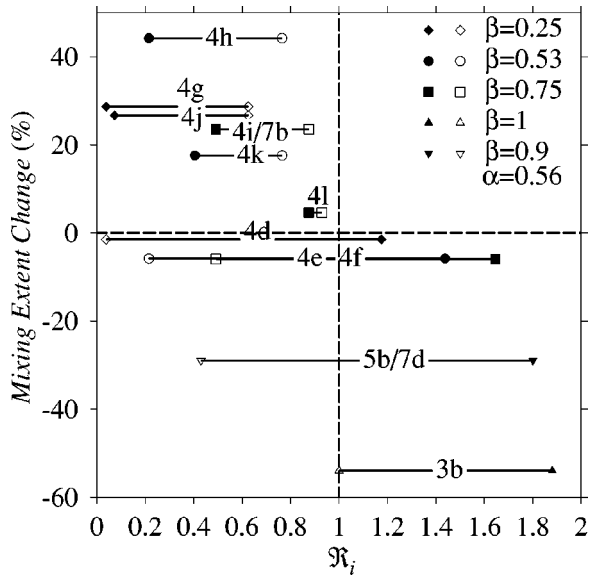

FIG. 6. Mixing extent variation of cohesive systems. The change in the extent of mixing is expected to be positive for values of $\Re_i < 1$ and negative for $\Re_i > 1$. Here we plot the values of the extent change and $\Re_i$ for experiments in Figs. 3–5.

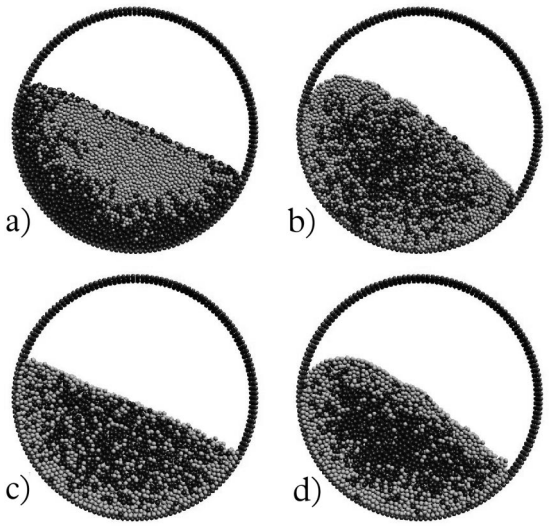

FIG. 7. Results from PD simulation. (a) Dry and (b) wet mixing results for varying particle size only [corresponds to a computational equivalent of Figs. 4(c)–4(i), respectively]. (c) Dry and (b) wet mixing results for varying size, density, and wetting angle [roughly equivalent to Figs. 5(a) and 5(b), respectively].

angle ratio as the experiments 5*b* (5*a*) (see Table I). As before, the asymptotic distribution for free-flowing (dry) particles represents only mild segregation [Fig. 7(c)], while the addition of interstitial moisture [Fig. 7(d)] again causes the particles to become more segregated, as predicted.

It should be pointed out that the method of *IS* calculation differs between the computations (which can probe the full three-dimensional flow) and the optical technique used for experiments (which is limited to surface and wall measurements). Nevertheless, there is a surprising degree of agreement between the simulated *IS* percentage changes between Figs. 7 and 4 or 5 (see Table II).

VI. CONCLUSION

In this work we examine the effect of a liquid-bridge induced cohesion force on particle mixing for flows dominated by gravity. We apply a recently developed characterization tool, Bo_g, to develop a model complete with phase diagrams which exhibit both mixed and segregated phases. Using this model we correctly predict, both qualitatively and quantitatively, the mixing and segregation at the asymptotic state for systems with constant moisture content, but varying particle properties. These results may support a method for controlling the mixing behavior of particle systems via manipulating the phase diagram (e.g., changing size or density ratios).

In this work we have expressly avoided the effect of both liquid-bridge viscosity [9] and volume [10,11] on mixing and segregation by varying only particle properties at constant water saturation. Clearly, for a more complete picture of the impact of interstitial moisture on generic particle mixing systems, these and other effects must be examined further.

ACKNOWLEDGMENTS

We thank Christos Karanikas, Derek Triplett, and Steve Nase for help with experimental setup. This work was supported by the Chemical and Transport Systems Division of the National Science Foundation and the Petroleum Research Fund, administered by the American Chemical Society.

[1] R. L. Brown, J. Inst. Fuel **13**, 15 (1939).
[2] J. C. Williams, Powder Technol. **15**, 245 (1976).
[3] H. M. Jaeger, J. B. Knight, and S. R. Nagel, Phys. Rev. Lett. **70**, 3728 (1993).
[4] O. Pouliquen, J. Delour, and S. B. Savage, Nature (London) **386**, 816 (1997).
[5] H. A. Makse, S. Havlin, P. R. King, and H. E. Stanley, Nature (London) **386**, 379 (1997).
[6] J. M. Ottino and D. V. Khakhar, Annu. Rev. Fluid Mech. **32**, 55 (2000).
[7] T. Mullin, Science **295**, 1851 (2002).
[8] J. J. McCarthy, D. V. Khakhar, and J. M. Ottino, Powder Technol. **109**, 72 (2000).
[9] A. Samadani and A. Kudrolli, Phys. Rev. Lett. **85**, 5102 (2000).
[10] A. Samadani and A. Kudrolli, Phys. Rev. E **64**, 051301 (2001).
[11] D. Geromichalos, M. Kohonen, F. Mugele, and S. Herminghaus, Phys. Rev. Lett. **90**, 168702 (2003).
[12] H. Li and J. J. McCarthy, Phys. Rev. Lett. **90**, 184301 (2003).

[13] R. Albert, I. Albert, D. Hornbaker, P. Schiffer, and A.-L. Barabási, Phys. Rev. E **56**, R6271 (1997).
[14] D. Hornbaker, R. Albert, I. Albert, A.-L. Barabási, and P. Schiffer, Nature (London) **387**, 765 (1997).
[15] T. C. Halsey and A. J. Levine, Phys. Rev. Lett. **80**, 3141 (1998).
[16] P. Pierrat and H. S. Caram, Powder Technol. **91**, 83 (1997).
[17] N. Harnby, *Mixing in the Process Industries*, edited by N. Harnby, M. F. Edwards, and A. W. Nienow (Butterworths Heineman Publishers, London, 1992), pp. 78–94.
[18] S. T. Nase, W. L. Vargas, A. A. Abatan, and J. J. McCarthy, Powder Technol. **116**, 214 (2001).
[19] S. Torquato, Nature (London) **405**, 521 (2000).
[20] D. V. Khakhar, J. J. McCarthy, T. Shinbrot, and J. M. Ottino, Phys. Fluids **9**, 31 (1997).
[21] C. M. Dury and G. H. Ristow, Phys. Fluids **11**, 1387 (1999).
[22] J. L. Lenhart *et al.*, J. Colloid Interface Sci. **221**, 75 (2000).
[23] D. V. Khakhar, A. V. Orpe, and S. K. Hajra, J. Phys. A **318**, 129 (2003).
[24] C. Thornton, Kona **15**, 81 (1997).
[25] C. Thornton, K. K. Yin, and M. J. Adams, J. Phys. D **29**, 424 (1996).
[26] D. V. Khakhar, J. J. McCarthy, and J. M. Ottino, Phys. Fluids **9**, 3600 (1997).
[27] P. A. Cundall and O. D. L. Strack, Geotechnique **29**, 47 (1979).
[28] K. L. Johnson, in *Contact Mechanics* (Cambridge University Press, Cambridge, England, 1987).
[29] G. Lian, C. Thornton, and M. J. Adams, J. Colloid Interface Sci. **161**, 138 (1993).
[30] G. Lian, C. Thornton, and M. J. Adams, Chem. Eng. Sci. **53**, 3381 (1998).
[31] T. Mikami, H. Kamiya, and M. Horio, Chem. Eng. Sci. **53**, 1927 (1998).
[32] M. J. Rhodes, X. S. Wang, M. Nguyen, P. Stewart, and K. Liffman, Chem. Eng. Sci. **56**, 4433 (2001).
[33] O. R. Walton, Mech. Mater. **16**, 239 (1993).